



Effects of nanoparticles on the tensile behavior of ultra-high-performance fiber-reinforced concrete at high strain rates

Van Phi Dang^{a,b}, Dong Joo Kim^{a,*}

^a Department of Civil and Environmental Engineering, Sejong University, 98 Gunja-dong, Gwangjin-gu, Seoul, 143-747, Republic of Korea

^b Department of Civil Engineering, Hanoi University of Mining and Geology, Hanoi, Viet Nam

ARTICLE INFO

Keywords:

Nanoparticles
Ultra-high-performance fiber-reinforced concrete
Tensile resistance
Rate sensitivity

ABSTRACT

This study investigated the effects of nanoparticles (NPs) on the tensile resistance of ultra-high-performance fiber-reinforced concrete (UHPFRC), containing 1.5 vol% smooth steel fibers, at both static (0.000167 s^{-1}) and high strain rates ($61.86\text{--}162.00 \text{ s}^{-1}$). Three types of NPs, namely nano- CaCO_3 (3 wt%), nano- SiO_2 (1 wt%), and nano-carbon nanotube (CNT) (1 wt%) were considered. All the UHPFRCs containing NPs generated higher rate-sensitive tensile resistance than the UHPFRCs without NPs. For instance, the dynamic increase factor (DIF) for the post-cracking strengths of the UHPFRCs containing nano- CaCO_3 , nano- SiO_2 , or nano-CNT was 2.94, 2.79, and 2.69, respectively, while that of the UHPFRCs without NPs was 2.65. The DIFs for tensile parameters of UHPFRCs were dependent upon the types of NPs: nano- CaCO_3 produced the highest DIFs for first- and post-cracking strengths, and the number of microcracks, whereas nano-CNT generated the highest DIFs for strain capacities and peak toughness. Besides, the sources of the rate sensitivity of tensile resistances of UHPFRCs containing NPs are closely related to the interfacial bond strengths and compressive strength of matrices.

1. Introduction

The frequency of blasts and other impacts caused by natural and man-made hazards has increased over the past two decades. Therefore, the demand for enhancing the resistance of engineering structures to impacts and blasts has increased [1–5]. Terrorist attacks and natural disasters, such as the 9/11 attack (2001), Moscow metro bombings (2010), Fukushima nuclear power plant disaster (2011), bombings at a market in the Baghdad governorate in Iraq (2021), and bombing at the Kabul International Airport in Afghanistan (2021), have resulted in the death of numerous people and led to substantial economic losses worldwide [1–8].

To mitigate the collapse of buildings and damage to infrastructure caused by such disasters, the development of high-performance construction materials with high tensile resistance and energy absorption capacity is increasingly researched [1,9–12]. Ultra-high-performance fiber-reinforced concrete (UHPFRC), which is a high-performance construction material, is typically composed of high-strength fibers and high-efficiency superplasticizer, exhibiting low water-to-binder ratio and high binder content [13–15]. Owing to a high packing density, UHPFRC has demonstrated significantly higher strength, durability, toughness, and energy absorption capacity than conventional concrete [1,12,16]. Although the packing density of UHPFRC is substantially higher than that of

Abbreviations: DIF, dynamic increase factor; FMZ, fiber–matrix zone; NPs, nanoparticles; UHPFRC, ultra-high-performance fiber-reinforced concrete.

* Corresponding author.

E-mail address: djkim75@sejong.ac.kr (D.J. Kim).

Table 1
Tensile parameters of matrices at high strain rates for FRCs and UHPFRCs.

Matrices	Testing machine	Fiber types	Fiber aspect ratio (L_f/d_f)	Strain rates	Fiber content	Matrix strength	First – cracking strength		Post – cracking strength		Strain capacity at post – cracking strength	Peak Toughness		Number of cracks		Average crack width	Reference		
				s^{-1}	vol%	MPa	MPa	DIF	MPa	DIF	%	DIF	kJ/m^3	DIF	ea	DIF	μm	DIF	
FRCs	MHB	Medium smooth steel fiber	80	300.00	1.25	80	–	–	8.62	2.81	–	–	–	–	–	–	–	Caverzan et al. [25]	
FRCs	I-SEFIM	Short smooth and hooked steel fibers	65, 80	53.00	1.0, 1.0	56	–	–	25.10	2.30	0.90	1.20	175.40	2.30	10	–	47	1.50	Park et al. [26]
FRCs	I-SEFIM	Short smooth and hooked steel fibers	65, 80	161.00	1.0, 1.0	81	–	–	24.10	2.10	2.40	3.70	383.20	6.00	10	–	118	3.60	Park et al. [26]
UHPFRCs	SEFIM	Long smooth steel fiber	100	22.42	1.00	180	–	–	16.52	2.18	1.99	3.21	179.63	4.18	–	–	–	–	Tran et al. [27]
UHPFRCs	SEFIM	Long smooth steel fiber and polyamide fiber	100, 1.14	24.86	1.0, 0.5	150	–	–	19.79	2.13	2.57	3.38	295.23	4.58	–	–	–	–	Tran et al. [27]
UHPFRCs	SEFIM	Long smooth steel fiber	100	21.40	1.50	180–200	–	–	37.10	3.30	1.00	1.50	239.70	3.80	–	–	–	–	Tran and Kim [28]
UHPFRCs	SEFIM	Medium smooth steel fiber	95	9.80	1.50	180–200	–	–	34.48	2.90	1.00	2.50	121.10	2.80	–	–	–	–	Tran and Kim [28]
UHPFRCs	SEFIM	Short smooth steel fiber	65	10.50	1.50	180–200	–	–	27.10	2.50	1.04	4.50	120.20	5.50	–	–	–	–	Tran and Kim [28]
UHPFRCs	M-SEFIM	Medium smooth steel fiber	125	127.10	1.00	150	14.60	2.40	25.30	3.10	0.82	2.50	248.70	7.20	–	–	–	–	Pyo et al. [29]
UHPFRCs	M-SEFIM	Medium smooth steel fiber	125	141.10	2.00	150	27.10	2.80	44.70	3.00	1.16	2.1	498.70	5.90	–	–	–	–	Pyo et al. [29]
UHPFRCs	I-SEFIM	Medium smooth and hooked steel fibers	95, 80	170.00	2.00	180	–	–	39.40	2.80	1.60	1.60	406.10	3.30	12	–	68	1.80	Park et al. [26]
UHPFRCs	SEFIM	Long smooth steel fiber	100	12.30	1.50	180	–	–	22.60	1.8	1.14	2.00	16.60	2.80	8	0.60	–	–	Tran et al. [1]
UHPFRCs	SEFIM	Short smooth steel fiber	65	16.50	1.50	180	–	–	19.20	1.8	1.10	2.80	12.50	3.30	5	1.10	–	–	Tran et al. [1]
UHPFRCs	I-SEFIM	Medium smooth steel fiber	95	32.00	1.50	180–200	–	–	23.06	1.90	0.54	1.70	66.62	2.00	5	2.50	–	–	Park et al. [30]
UHPFRCs	I-SEFIM	Medium smooth steel fiber	95	140.00	2.00	180–200	–	–	44.72	2.70	1.78	2.10	455.56	4.00	27	3.00	–	–	Park et al. [30]

Modified Hopkinson bar (MHB); Strain energy frame impact machine (SEFIM); Improved strain energy frame impact machine (I-SEFIM); Modified impact testing system (M-SEFIM).
 L_f : length of the fiber; d_f : diameter of the fiber.

normal concrete or fiber-reinforced concrete (FRC), a relatively weak fiber–matrix zone (FMZ) exists between the fiber and matrix [17, 18].

In general, the mechanical properties of UHPFRC are known to be influenced by the properties of the FMZ. Therefore, several researchers have investigated the effects of nanoparticles (NPs) on the properties of FMZ and the mechanical resistance of UHPFRC to increase its strength and energy absorption capacity [14,15,19–23]. The addition of 3.2% nano-CaCO₃ to UHPFRC significantly increases the maximum bond strength and pullout energy of steel fibers embedded in UHPFRC by 45 and 200%, respectively [13,14]. Furthermore, Li et al. [19] reported that the addition of 3 wt% nano-CaCO₃ to UHPFRC enhanced their compressive and flexural strengths by 8 and 20%, respectively. Wille and Loh [20] reported that the maximum pullout resistance of steel fibers embedded in UHPFRC was enhanced by 40% owing to the addition of 0.022 wt% multi-walled carbon nanotubes (MWCNTs).

Several researchers have investigated the effects of NPs on the tensile behavior of UHPFRC at static strain rates [21,24]. Liu et al. [21] investigated the effect of nano-CaCO₃ content ranging from 1 to 4 wt% on the tensile resistance of UHPFRC at a static strain rate of 0.000104 s⁻¹. They reported that the addition of 3% nano-CaCO₃ produces the highest tensile strength of UHPFRC (15 MPa), whereas excessive content of 4% nano-CaCO₃ exhibits a negligible effect on the tensile strength of UHPFRC owing to agglomeration concerns. Furthermore, Shaikh et al. [24] examined the influence of a mixture of fly ash contents (20–50 wt%) and nano-SiO₂ (2 wt%) on the tensile strength of UHPFRC at a static strain rate (0.000104 s⁻¹). They reported that the tensile strength of UHPFRC containing the mixture of fly ash and nano-SiO₂ decreased by 14–19%. Additionally, their results demonstrated that the tensile strength of UHPFRC containing nano-SiO₂ (2 wt%) was 32% lower than that of UHPFRC without nano-SiO₂. Although researchers have tried to improve the mechanical properties of UHPFRC at static rates by containing various types of NPs, the effects of NPs on the tensile behavior of UHPFRC, particularly at high strain rates, are not sufficiently explored. Furthermore, at high strain rates, the correlation between the interfacial bond strength and tensile resistance of UHPFRCs containing NPs requires further clarity.

Most existing studies have focused only on the tensile behavior of UHPFRC using different matrix strengths, fiber types, and fiber volume contents. Table 1 summarizes the tensile characteristics of FRC and UHPFRC with different matrix strengths, fiber contents, and fiber types of smooth steel fibers or combinations of smooth steel fibers and other fibers at high strain rates [1,25–30]. Park et al. [30] reported that the improvements in the post-cracking strength (σ_{pc}), strain capacity at the post-cracking strength (ϵ_{pc}), peak toughness (T_p), and the number of microcracks (n_{cr}) of UHPFRC with lower smooth steel fiber volume content (1.5%) were higher than those of UHPFRC with higher smooth steel fiber volume content (2.0%), owing to the group effects of fibers. Additionally, Tran et al. [1] reported that UHPFRC with long smooth steel fibers resulted in higher enhancement of σ_{pc} than UHPFRC with medium smooth steel fibers at identical fiber volume contents (1.5%); however, UHPFRCs with medium smooth steel fibers generated higher dynamic increase factors (DIFs) for the T_p , ϵ_{pc} , and n_{cr} of UHPFRCs than those with long smooth steel fibers owing to the effects of both crack widths and the number of cracks. Although the tensile behavior of UHPFRCs at high strain rates has been investigated, the source of the enhancement in tensile resistance of UHPFRC still remains unclear. According to the information provided, there is a lack of systematic evidence on the efficiency of NPs in improving the tensile resistance of UHPFRC at high strain rates.

This study aims to address the lack of experimental evidence on the effect of NPs on the rate-sensitive tensile response of UHPFRC. The addition of NPs to UHPFRC is expected to enhance the tensile resistance of UHPFRC owing to the enhancement of the pullout

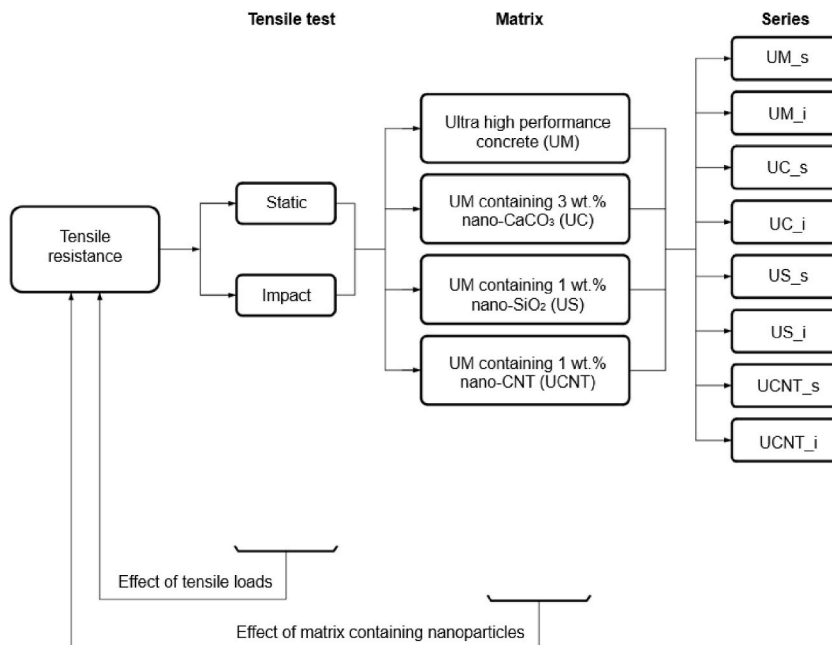


Fig. 1. Experimental system.

resistance of the fibers embedded in ultra-high-performance concrete (UHPC). Besides, as strain rates increased, UHPFRCs containing NPs are expected higher rate sensitivity for interfacial bond strengths, resulting in the tensile resistances of UHPFRCs containing NPs would be higher rate sensitive. The objective of this study is to evaluate the effects of NPs on the rate-sensitive tensile resistance of UHPFRC. The primary experimental variables included three types of NPs, namely nano-CaCO₃, nano-SiO₂, and nano-CNT, and the strain rate. Moreover, the source of the enhanced tensile resistance of UHPFRC at high strain rates is explored.

2. Experimental system

Fig. 1 illustrates the experimental system designed to investigate the effects of NPs on the tensile behavior of UHPFRC. Four matrices were used in this study, namely the ultra-high-performance concrete matrix (UM), UM containing 3% nano-CaCO₃ (UC), UM containing 1% nano-SiO₂ (US), and UM containing 1% nano-CNT (UCNT). The mass ratio of cementitious materials was used to determine the volume content of the NPs. Additionally, the four matrices comprised the same 1.5% long smooth steel fiber volume content.

2.1. Materials and specimen preparation

Table 2 summarizes the properties of the matrices, and Table 3 lists the properties of the long smooth steel fibers. The matrices considered in this study comprise the following components: Type I cement, nano-CaCO₃ (98.0% CaCO₃) with an average size of 50 nm, nano-SiO₂ (99.9% SiO₂) with a primary particle size of 50 nm, MWCNT with a diameter of 200 nm and length 10 μm, silica sand with grain size ranging from 210 to 250 μm, silica fume (98.5% SiO₂) with particles ranging from 0.1 to 1.0 μm, and silica powder containing 98.0% SiO₂ with an average particle size of 10 μm and a density of 2.6 g/m³. Furthermore, polycarboxylate ether superplasticizers (SPs) with a solid content of 30% were used to increase matrix workability.

The matrices were prepared using a Hobart-type mixer. During the initial 5 min, dry components such as sand, silica powder, silica fume, and cement were dry-mixed. After dry mixing, water was added gradually for approximately 1 min to prepare the UM mixture, which was continuously mixed for approximately 5 min. Subsequently, SP was gradually poured, and the mixture was mixed further for approximately 5 min.

Mixtures containing NPs were prepared as follows [31]: (1) a sonicator with a cycle of 15 s and an amplitude of 50% was used to distribute the NPs in the solution containing water and half the amount of SP for approximately 2 h; (2) sand, silica powder, silica fume, and cement were initially mixed for approximately 5 min; (3) the solution containing water, NPs, and SP was gradually added for approximately 2 min; and (4) the remaining amount of SP was gradually added into the mixture and mixed for approximately 5 min. Finally, long smooth steel fibers were added and carefully distributed by hand into the mixtures. The mixtures were continuously mixed when the fibers were added individually to the mixes. After adding all the fibers to the mixtures, they were further mixed for 2 min before terminating the mixing procedure.

The mixtures with fibers were poured into molds using a wide scoop with slight vibrations. All specimens were maintained at 20 ± 2 °C for 48 h before demolding. Subsequently, the specimens were placed in a hot water tank at 90 ± 2 °C for three days and tested after 28 days. Before testing, the specimens were sprayed with three coats of polyurethane on their surfaces to ensure easy detection of cracks [26].

Fig. 2 depicts the specimen geometries for both the static and impact tests. During tensile tests, failure outside the gauge length of the specimens must be prevented. Therefore, two layers of a steel wire mesh were strengthened at both ends of the specimens (Fig. 2a and b) [10]. Unlike the specimens used in the static tests, the specimens for the impact tests were created by cutting off one bell-shaped end with a longer wire mesh, which was then directly linked to the transmitter bar via a connector (Fig. 2b). Fig. 2c depicts the cross-section of the tensile specimens in the gauge length area with the dimensions of 50 mm × 25 mm. The gauge length was maintained at 100 mm for both static and impact tests to ensure consistency of the specimens used [10]. Thus, the wire mesh on one bell-shaped end was lengthened to two ends of the specimens. Besides, the wire mesh ensured that failures during testing occur only within the gauge length of specimens, as depicted in Fig. 2a and b.

2.2. Test setup and procedure

Fig. 3 depicts the universal testing machine (UTM) used to perform the static tensile tests. The load was maintained at a speed of 1 mm/min, which was equivalent to a strain rate of 0.000167 s⁻¹. The boundary conditions for both ends of the specimens were hinge-to-hinge connections, which were suitable for examining the tensile behaviors of strain-hardening fiber cementitious composites [32]. During the test, the elongation of the specimens within the gauge length range was measured using two linear variable differential transformers (LVDTs) attached to the specimens, and tensile loads were obtained from a load cell placed on top of the specimens

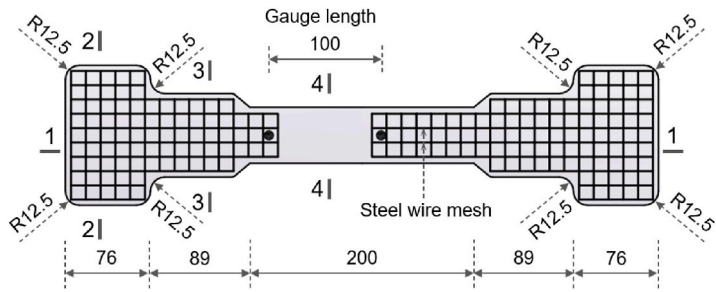
Table 2
Matrix composition in terms of weight ratio and compressive strength.

Matrix type	Cement (Type I)	Nano-CaCO ₃	Nano-SiO ₂	Nano-CNT	Silica sand	Silica fume	Silica powder	SP	W/C	Compressive strength (MPa)	Flow test (mm)
UM	1.00	–	–	–	1.1	0.25	0.3	0.075	0.2	186.8	220
UC	0.97	0.03	–	–	1.1	0.25	0.3	0.075	0.2	206.2	165
US	0.99	–	0.01	–	1.1	0.25	0.3	0.075	0.2	201.4	175
UCNT	0.99	–	–	0.01	1.1	0.25	0.3	0.075	0.2	188.9	170

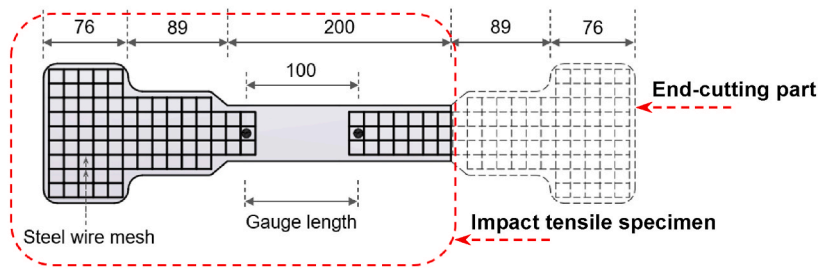
Nano-CNT: Multi-walled carbon nanotube; SP: Superplasticizer; W/C: Water-to-cement ratio.

Table 3
Properties of straight smooth steel fibers.

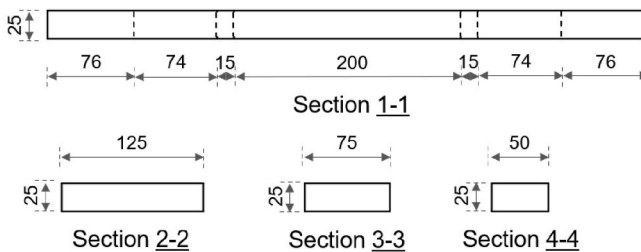
Diameter (mm)	Length (mm)	Density (g/cm ³)	Tensile strength (MPa)	Elastic modulus (GPa)	Material
0.3	30	7.9	2447	200	Brass-coated high-strength steel fibers



(a) Static tensile specimen



(b) Impact tensile specimen



(c) Sections of the tensile specimen

Fig. 2. Geometry of tensile specimens (unit: mm).

(Fig. 3).

Fig. 4 illustrates the detailed test setup for the impact tensile tests. A strain energy frame impact machine (SEFIM) with high strain rates (5–19 s⁻¹) was initially developed by Tran and Kim [33]. Subsequently, Park et al. [30] developed an improved SEFIM (I-SEFIM) with higher strain rates (10–150 s⁻¹) based on the SEFIM system. In this study, the I-SEFIM system was employed to investigate the tensile behavior of the matrices at high strain rates. The impact tensile test procedure is described in detail in previous studies [1,10,30,33]. Fig. 4a depicts the I-SEFIM, prior to testing, a coupler was used to link the energy frames to the pullout bar of a hydraulic jack system. The movement of energy frames is hindered by the fixed support 3 (Part 16 in Fig. 4a). Subsequently, a tensile specimen was placed in I-SEFIM, wherein one end of the specimen is placed on a connector with a hinged grip system, whereas the other end is linked to a transmitter bar that is prevented from movement by fixed support [10,33].

A coupler with a capacity of 1960 kN was used in this study. The coupler was pulled by the hydraulic jack system until over the

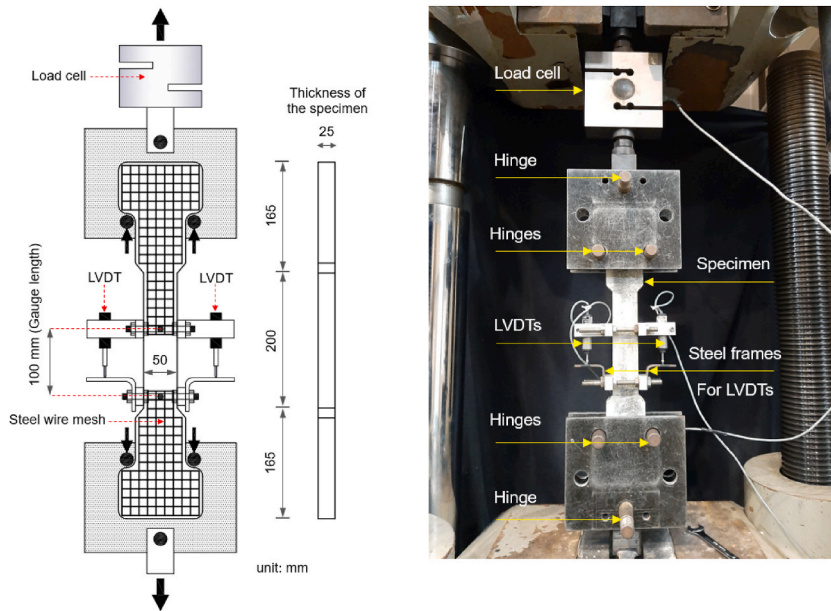


Fig. 3. Specimen geometry and test setup for static tensile tests.

maximum capacity of the coupler, and elastic strain energy stored within the energy frames generated a rapid stress wave inside the frames immediately after the failure of the coupler. The wave propagated through a grip to an impact tensile specimen and eventually failed the specimen [10,33].

As detailed in Fig. 4b, during impact tests, a high-speed camera was used to determine the elongation of the specimens by analyzing the sequential images of points 1 and 2 within the gauge length range. Furthermore, the tensile stress was averaged from two stress histories obtained from two strain gauges attached at both sides of a transmitter bar.

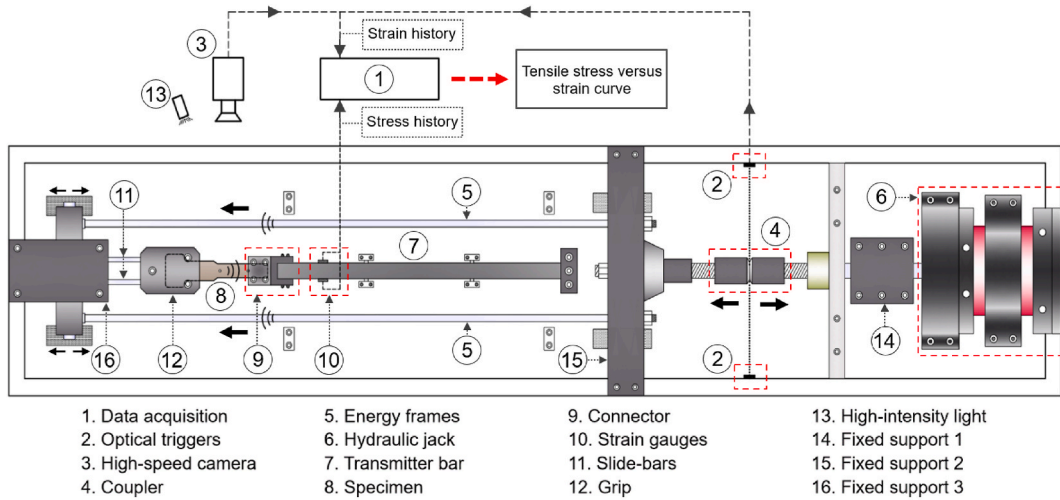
3. Test results

Fig. 5 depicts typical tensile stress versus strain curves of UHPFRC and their tensile parameters. The tensile parameters can be defined as follows [10]: first-cracking strength (σ_{cc}) is the stress at the first-cracking point; post-cracking strength (σ_{pc}) is the peak stress versus strain curve; ϵ_{cc} and ϵ_{pc} denote the strain capacities corresponding to the first- and post-cracking strengths, respectively; and the peak toughness (T_p) is defined as the area under the tensile stress and strain curve up to the highest stress. The number of microcracks (n_{cr}) was counted on both the front and back surfaces of the specimens along a gauge length of 100 mm; the average of the results was considered.

3.1. Static tensile test results

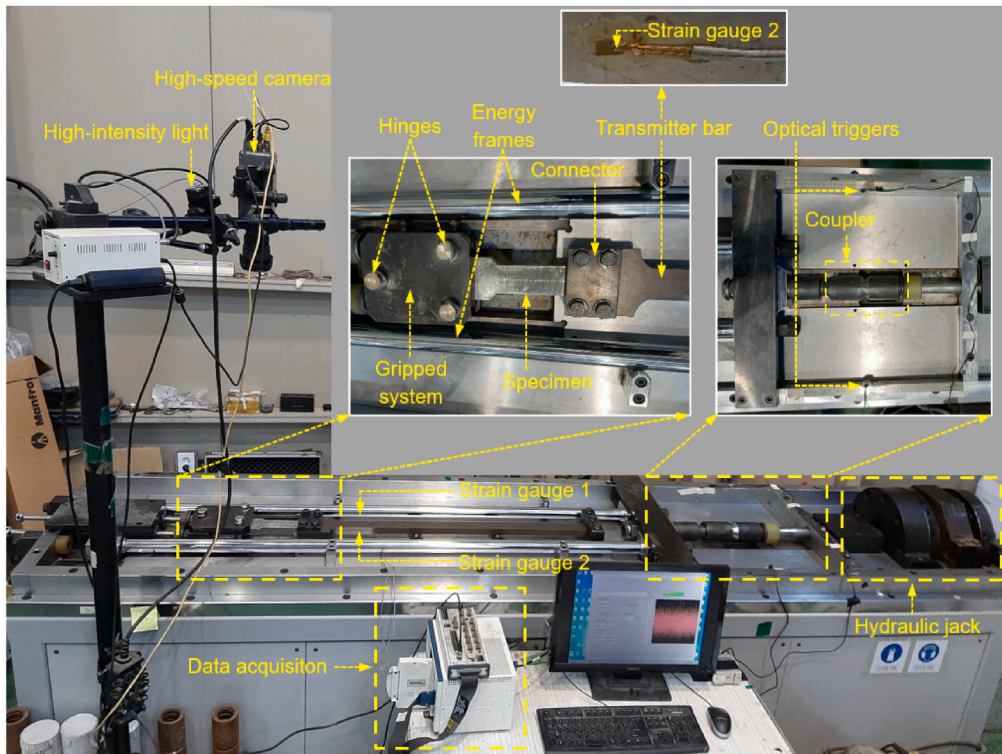
Fig. 6 illustrates the tensile stress versus strain curves corresponding to the UM, UC, US, and UCNT matrices at a static strain rate of 0.000167 s^{-1} . Table 4 lists the tensile parameters of the matrices at this static strain rate. The obtained test results indicate that the addition of NPs, including nano- CaCO_3 (3 wt%), nano- SiO_2 (1 wt%), and nano-CNT (1 wt%) to UHPFRC produces higher tensile strength in comparison with UHPFRC without any NPs; however, the tensile behavior of the matrices differed according to the types of NPs. For instance, the post-cracking strengths of UC, US, and UCNT matrices at the static strain rate increased by 34.07, 29.98, and 5.81%, respectively, compared to that of the UM matrix. This enhancement in the post-cracking strength of the UC matrix concurs with the findings reported by Liu et al. [21]; they reported that the post-cracking strength of UHPFRC containing nano- CaCO_3 (3 wt%) at a static strain rate of 0.000104 s^{-1} significantly increased by 40%. The improvement in the tensile resistance in matrices containing NPs can be attributed to the enhancement of the bond characteristics and the matrix strength [10,21,26].

Shaikh et al. [24] reported that the tensile strength of UHPFRC containing nano- SiO_2 (2 wt%) was lower than that of UHPFRC without nano- SiO_2 ; however, our investigation of the effect of nano- SiO_2 (1 wt%) on the tensile strength of UHPFRC contradicts these findings. This contradiction can be attributed to the content of nano- SiO_2 , which was added to UHPFRC. In our study, the tensile strength of UHPFRC containing 1 wt% nano- SiO_2 was higher than that of UHPFRC without nano- SiO_2 . The tensile strength of US matrix was 16.62 MPa while that of UM matrix was 13.66 MPa, as provided in Table 4. Although nano- SiO_2 could increase the mechanical properties of matrices, UHPFRCs containing the excessive content of nano- SiO_2 decreased their mechanical properties owing to the agglomeration of nano- SiO_2 [14,34]. Wu et al. [22] indicated that the optimal dosages of nano- SiO_2 to improve the compressive and flexural strengths of UHPFRCs were 0.5–1.5%. In addition, Wu et al. [14] reported that agglomeration problems caused by an excessive amount of nano- SiO_2 increase the porosity of the FMZ of UHPFRC, which reduces the bond strength of UHPFRC. Additionally, Kong et al. [34] reported that the aggregation of nano- SiO_2 resulted in the formation of weak zones inside the structure of the matrices,



- | | | | |
|----------------------|--------------------|-------------------|--------------------------|
| 1. Data acquisition | 5. Energy frames | 9. Connector | 13. High-intensity light |
| 2. Optical triggers | 6. Hydraulic jack | 10. Strain gauges | 14. Fixed support 1 |
| 3. High-speed camera | 7. Transmitter bar | 11. Slide-bars | 15. Fixed support 2 |
| 4. Coupler | 8. Specimen | 12. Grip | 16. Fixed support 3 |

(a) Detailed procedure of I-SEFIM



(b) I-SEFIM

Fig. 4. Detailed test setup for impact tensile tests using the improved strain energy frame impact machine (I-SEFIM).

which ultimately resulted in matrices with low strength and elastic modulus.

Fig. 7 compares the tensile parameters of four matrices including UM, UC, US, and UCNT at both static and high strain rates. At static strain rates (0.000167 s^{-1}), the tensile parameters of all matrices containing NPs (UC, US, and UCNT) generally were higher than those of UM. As depicted in Fig. 7a, the first-cracking strength (σ_{cc}) of UM, UC, US, and UCNT matrices were 7.69 ± 0.39 , 12.59 ± 1.05 , 10.83 ± 1.51 , and 8.65 ± 0.46 MPa, respectively. The σ_{cc} has been defined as the stress at first cracking and is mainly dependent upon the compressive strength of matrices [10,35]. The σ_{cc} of matrices containing NPs was higher than that of UM matrix because the UC, US, and UCNT produced a higher compressive strength in comparison with UM. The compressive strength of UC, US, UCNT, and UM was 206.2, 201.4, 188.9, and 186.8 MPa, respectively, as provided in Table 2.

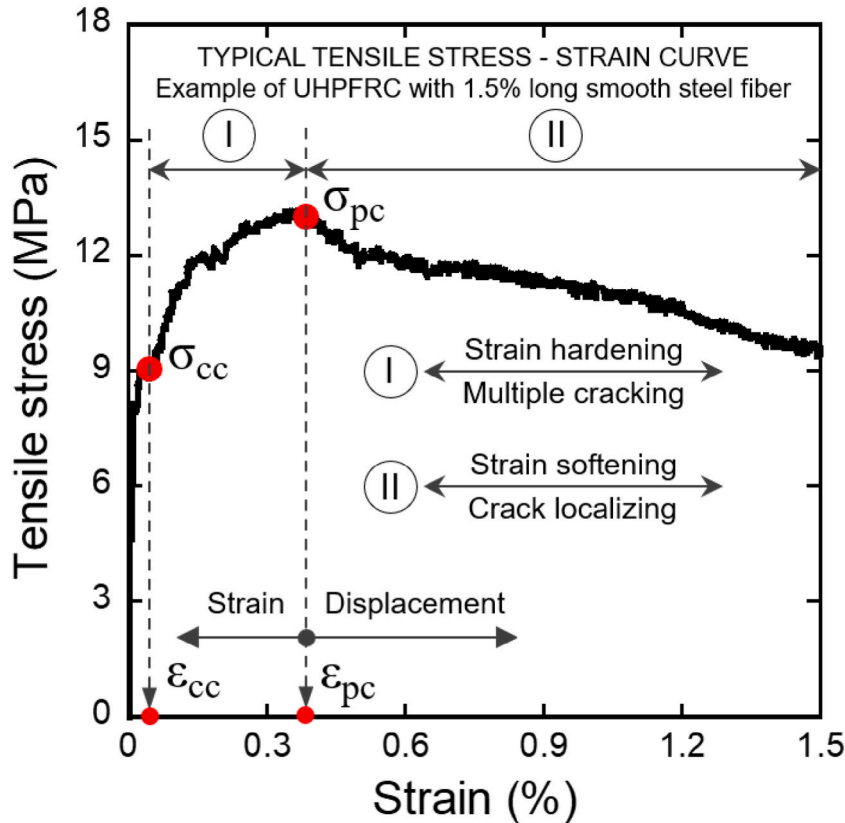


Fig. 5. Typical tensile stress–strain curve of ultra-high-performance fiber-reinforced concrete (UHPRFC) containing long smooth steel fibers.

The post-cracking strength (σ_{pc}), strain capacity (ϵ_{cc}), and peak toughness (T_p) are primarily dependent upon the interfacial bond strength [10]. The values of σ_{pc} of UM, UC, US, and UCNT matrices were 13.23 ± 0.44 , 17.73 ± 0.48 , 17.19 ± 0.44 , and 13.99 ± 0.41 MPa, respectively (Fig. 7b). Fig. 7c indicates that the values of ϵ_{cc} of UM, UC, US, and UCNT matrices were 0.34 ± 0.03 , 0.46 ± 0.16 , 0.44 ± 0.02 , and $0.37 \pm 0.11\%$, respectively. The values of T_p of UM, UC, US, and UCNT matrices were 55.49 ± 4.25 , 131.84 ± 33.31 , 89.13 ± 18.06 , and 83.58 ± 20.60 kJ/m³, respectively (Fig. 7d). The addition of NPs (nano-CaCO₃, nano-SiO₂, and nano-CNTs) significantly increased the interfacial bond strength of matrices leading to the improvement of the tensile parameters of the matrices containing NPs [36].

The addition of nano-CaCO₃ and nano-SiO₂ improved the microstructure and C–S–H content which significantly increased the adhesion and friction of straight fiber embedded in matrices [14,22]. However, that of nano-CNTs improved the packing density of matrices due to the filling effects but did not increase C–S–H content [20,37–39]. Besides, the addition of nano-CaCO₃, nano-SiO₂, and nano-CNTs to UHPRFCs significantly enhanced the hardness (H) of a fiber matrix zone (FMZ) surrounding fibers and matrix [48]. The effects of H on the interfacial bond strength of matrices would be further addressed in Section 4.2.1.

Additionally, all the matrices exhibited strain-hardening tensile behavior at a static rate with multiple cracks, as depicted in Fig. 8. The average numbers of cracks corresponding to the specimens of UM, UC, US, and UCNT were 6.20 ± 0.75 , 9.60 ± 1.02 , 8.50 ± 1.12 , and 7.60 ± 0.80 , respectively (Fig. 7e). The specimens of UC, US, and UCNT exhibited multiple discontinuous cracks along their gauge lengths whereas the specimens of UM generated multiple continuous cracks, as shown in Fig. 8. This phenomenon could be attributed to the effects of NPs on both compressive strength and interfacial bond strength of matrices [9,26]. The average value of crack widths of UC, US, and UCNT was smaller than that of UM because all matrices containing NPs produced higher multiple fine cracks in comparison with UM matrix, as shown in Fig. 8. The crack widths corresponding to UC, US, UCNT, and UM were 48, 52, 49, and 55 μ m, respectively, as provided in Table 4.

3.2. Impact tensile test results

Fig. 9 depicts the tensile stress versus strain curves of the matrices at high strain rates of 61.86–162.00 s⁻¹. Despite the identical test series, different strain rates were observed in the slightly different notch section areas of the couplers owing to manufacturing errors and inhomogeneous material properties that occurred during the specimen casting process [1].

Table 5 lists the tensile response parameters of the UM, UC, US, and UCNT matrices at high strain rates. Herein, the post-cracking strength of the UHPRFCs containing NPs was higher than that of the UM matrix. The post-cracking strengths of UC, US, and UCNT matrices increased by 48.53, 36.65, and 7.15%, respectively, compared to that of the UM matrix. Section 4 explains the reason for the

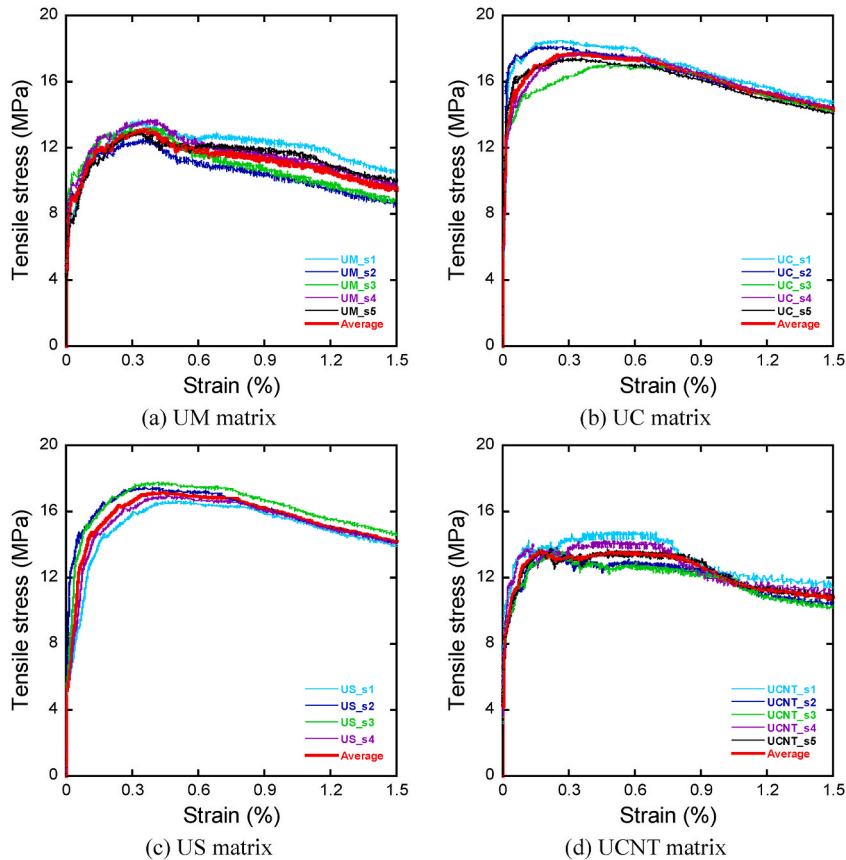


Fig. 6. Tensile stress versus strain response of the matrices at a specific static strain rate.

improvement in the tensile resistance of UHPFRC at high strain rates.

At high strain rates, the effects of NPs on the tensile resistances of matrices are also examined as demonstrated in Fig. 7. All matrices containing NPs generated higher first- and post-cracking strengths in comparison with UM matrix without NPs although the improvement of the tensile resistances of the matrices was different according to different NPs. At the high strain rates, the σ_{cc} of UM, UC, US, and UCNT matrices were 13.79 ± 1.12 , 23.48 ± 1.36 , 19.79 ± 0.69 , and 15.68 ± 0.76 MPa, respectively, while the σ_{pc} of UM, UC, US, and UCNT matrices were 35.10 ± 0.60 , 52.13 ± 1.22 , 47.96 ± 2.19 , and 37.61 ± 0.45 MPa, respectively, as shown in Fig. 7a and b. The improvement of the σ_{cc} and σ_{pc} of matrices containing NPs would be owing to the increased compressive strength and interfacial bond strength of matrices [10,35]. Among nano- CaCO_3 , nano- SiO_2 , and nano-CNT, nano- CaCO_3 produced the highest in both compressive strength and interfacial bond strength of matrices, whereas nano-CNT exhibited the lowest ones. The compressive strength of UC, US, and UCNT matrices was 206.2, 201.4, and 188.9 MPa, respectively, as provided in Table 2, while the equivalent bond strength of these matrices was 28.27, 24.36, and 16.79 MPa, respectively, as listed in Table 6.

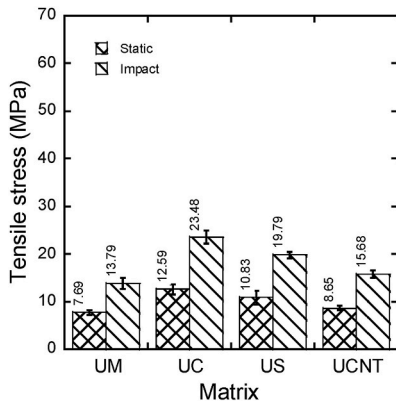
At the high strain rates, UHPFRCs containing NPs exhibited lower strain capacity than the UM matrix. The values of ϵ_{cc} of UM, UC, US, and UCNT matrices were 1.02 ± 0.16 , 0.92 ± 0.11 , 0.96 ± 0.17 , and $1.01 \pm 0.04\%$, respectively (Fig. 7c). The lower strain capacity of matrices containing NPs can be attributed to the varied cracking tendencies of the UHPFRC containing NPs at high strain rates. For instance, although UC produced numerous micro-cracks, the crack openings or crack widths ($49 \mu\text{m}$) were substantially smaller than those observed in UM ($93 \mu\text{m}$). Consequently, the UC matrix generated a significantly less strain capacity at high strain rates than the UM matrix.

In addition, the UC, US, and UCNT matrices produced higher peak toughness (T_p) than UM matrix. The values of T_p of UM, UC, US, and UCNT matrices were 448.50 ± 68.02 , 587.78 ± 69.56 , 553.96 ± 54.72 , $539.77 \pm 4.51 \text{ kJ/m}^3$, respectively, as shown in Fig. 7d. The improvement of the T_p of matrices containing NPs was primarily dependent upon the interfacial bond strength [10]. The interfacial bond strength between the fibers and matrix in the UHPFRC containing NPs significantly increased owing to the enhancement of the C-S-H content and filling effects of the NPs [15,22,23]. At high strain rates, the UC matrix exhibited higher tensile resistance than the US and UCNT matrices because nano- CaCO_3 produced higher interfacial bond strength in UHPFRC than nano- SiO_2 and nano-CNT (would be discussed in Section 4). Furthermore, nano- CaCO_3 chemically reacts with tricalcium aluminate (C_3A), resulting in increased precipitation of reaction products on the surface of steel fibers [22,23]. However, nano-CNT generates only a high packing density owing to the filling effects on the microstructure of the UM matrix [37–39].

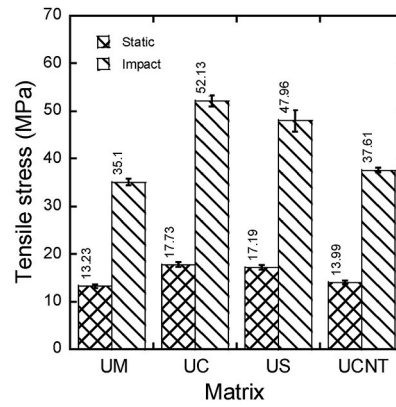
Additionally, all matrices exhibited strain-hardening behavior accompanied by multiple micro-cracks at high strain rates (Fig. 10).

Table 4
Tensile parameters of matrices at a specific static strain rate.

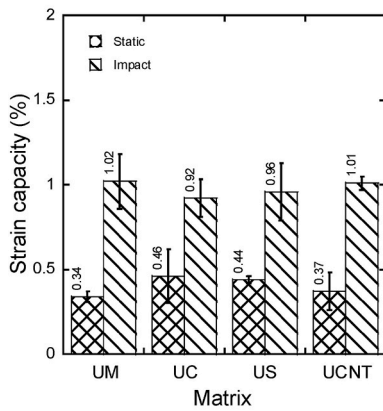
Series		Strain rate		First-cracking strength		Post-cracking strength		Strain capacity		Peak toughness		Number of cracks		Average crack width	
		Type	s ⁻¹	MPa	DIF	MPa	DIF	%	DIF	kJ/m ³	DIF	ea	DIF	μm	DIF
UM	UM_s1	Static	0.000167	7.24	–	13.66	–	0.33	–	51.18	–	6.00	–	55	–
	UM_s2	–	–	8.35	–	12.49	–	0.36	–	56.84	–	7.00	–	52	–
	UM_s3	–	–	7.44	–	13.25	–	0.30	–	55.60	–	7.00	–	43	–
	UM_s4	–	–	7.85	–	13.68	–	0.37	–	62.64	–	6.00	–	62	–
	UM_s5	–	–	7.56	–	13.05	–	0.33	–	51.18	–	5.00	–	66	–
	Average	■	■	7.69	1.00	13.23	1.00	0.34	1.00	55.49	1.00	6.20	1.00	55	1.00
UC	UC_s1	Static	0.000167	13.84	–	18.36	–	0.27	–	89.53	–	11.00	–	25	–
	UC_s2	–	–	13.91	–	18.13	–	0.30	–	100.71	–	10.00	–	30	–
	UC_s3	–	–	11.82	–	17.03	–	0.70	–	179.42	–	8.00	–	87	–
	UC_s4	–	–	11.74	–	17.75	–	0.56	–	152.91	–	10.00	–	56	–
	UC_s5	–	–	11.66	–	17.38	–	0.49	–	136.60	–	9.00	–	54	–
	Average	■	■	12.59	1.00	17.73	1.00	0.46	1.00	131.84	1.00	9.60	1.00	48	1.00
US	US_s1	Static	0.000167	8.30	–	16.62	–	0.44	–	60.27	–	9.00	–	49	–
	US_s2	–	–	12.00	–	17.46	–	0.44	–	87.52	–	8.00	–	55	–
	US_s3	–	–	12.00	–	17.75	–	0.42	–	102.81	–	7.00	–	60	–
	US_s4	–	–	11.00	–	16.92	–	0.46	–	105.93	–	10.00	–	46	–
	Average	■	■	10.83	1.00	17.19	1.00	0.44	1.00	89.13	1.00	8.50	1.00	52	1.00
	UCNT	UCNT_s1	Static	0.000167	9.29	–	14.72	–	0.46	–	107.69	–	7.00	–	66
UCNT_s2		–	–	8.52	–	13.66	–	0.27	–	65.55	–	8.00	–	34	–
UCNT_s3		–	–	8.06	–	13.66	–	0.30	–	71.80	–	9.00	–	33	–
UCNT_s4		–	–	9.06	–	14.20	–	0.55	–	109.46	–	7.00	–	78	–
UCNT_s5		–	–	8.30	–	13.74	–	0.26	–	63.38	–	7.00	–	38	–
Average		■	■	8.65	1.00	13.99	1.00	0.37	1.00	83.58	1.00	7.60	1.00	49	1.00



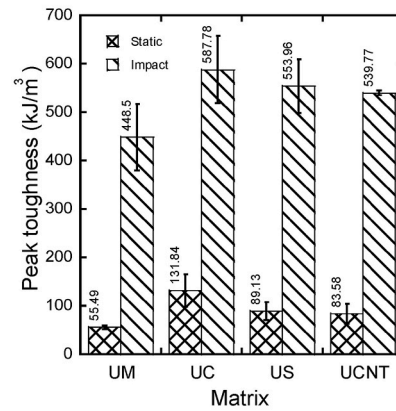
(a) First-cracking strength



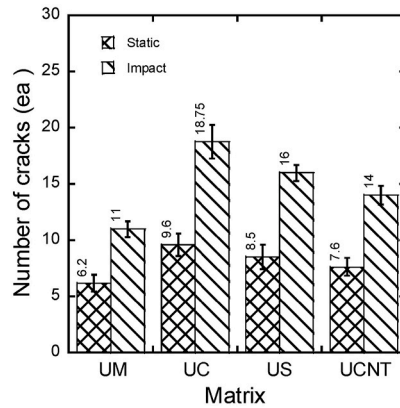
(b) Post-cracking strength



(c) Strain capacity



(d) Peak toughness



(e) Number of cracks

Fig. 7. Effect of nanoparticle types on the tensile resistances of the ultra-high-performance fiber-reinforced concrete (UHPFRC).

Although UHPFRCs containing NPs produced higher numbers of cracks in comparison to UM matrix, UHPFRCs containing NPs generated lower crack widths than UM matrix. The average numbers of cracks of UM, UC, US, and UCNT matrices were 11.00 ± 0.71 , 18.75 ± 1.48 , 16.00 ± 0.71 , and 14.00 ± 0.82 , respectively (Fig. 7e), whereas the crack widths of the matrices were 93, 49, 60, and 72 μm , respectively (Table 5).

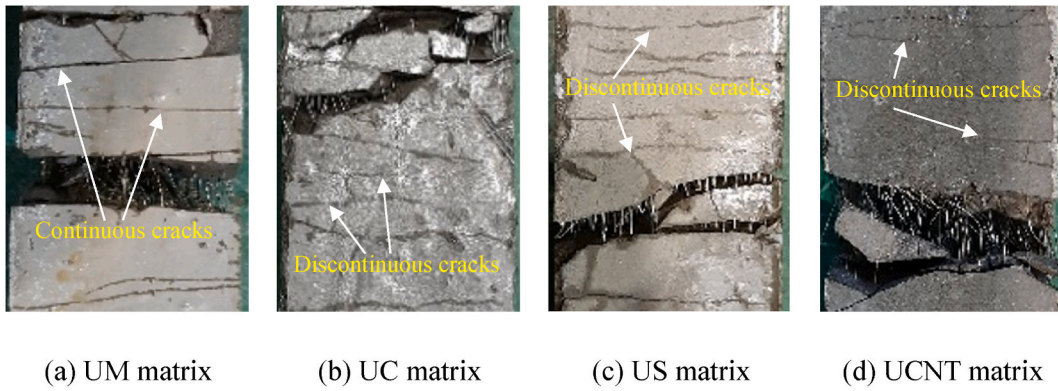


Fig. 8. Multiple cracking behaviors within the gauge length of matrices at a static rate.

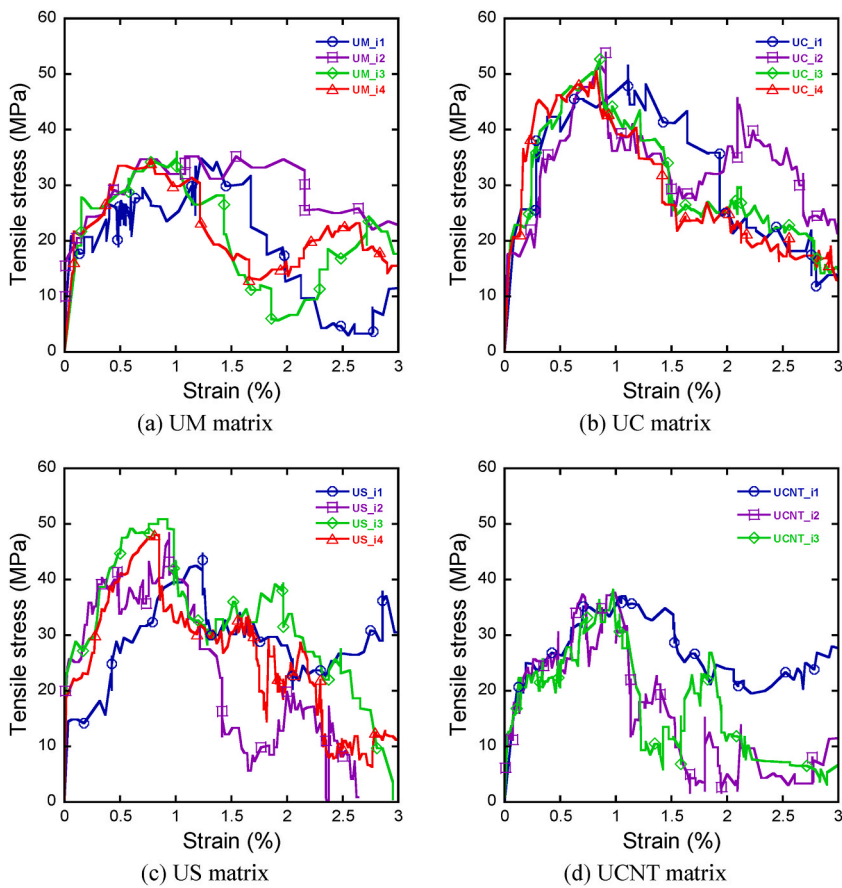


Fig. 9. Tensile stress versus strain responses of matrices at high strain rates.

3.3. Strain rate sensitivity

The tensile parameters of the matrices were sensitive to the applied strain rates between the static strain rate (0.000167 s^{-1}) and high strain rates ($61.86\text{--}162.00 \text{ s}^{-1}$). DIF is defined as the ratio of dynamic to static characteristics; Table 5 indicates that the DIFs of the first- and post-cracking strengths of the matrices ranged from 1.57 to 2.03 and 2.60 to 3.03, respectively. Furthermore, DIFs of the strain capacity, peak toughness, and number of cracks of the matrices ranged between 1.78 and 3.61, 4.07 and 9.16, and 1.57 and 2.25, respectively (Table 5).

Fig. 11 illustrates the curves used for forecasting the DIFs of the tensile strength of normal concrete and UHPFRC proposed by the Euro-International Committee for Concrete and the International Federation for Pre-stressing (CEB-FIP) model [40], Malvar and Ross

Table 5
Tensile parameters of matrices at high strain rates.

Series		Strain rate		First-cracking strength		Post-cracking strength		Strain capacity		Peak toughness		Number of cracks		Average crack width	
		Type	s ⁻¹	MPa	DIF	MPa	DIF	%	DIF	kJ/m ³	DIF	ea	DIF	μm	DIF
UM	UM_i1	Impact	61.86	14.39	1.87	34.77	2.63	1.22	3.61	508.06	9.16	11.00	1.77	111	2.03
	UM_i2	–	72.39	12.03	1.57	35.21	2.66	1.08	3.20	496.64	8.95	12.00	1.94	90	1.65
	UM_i3	–	93.86	13.71	1.78	36.01	2.72	1.01	2.97	453.14	8.17	11.00	1.77	91	1.67
	UM_i4	–	124.71	15.02	1.95	34.40	2.60	0.77	2.28	336.16	6.06	10.00	1.61	77	1.41
	Average	–	88.20	13.79	1.79	35.10	2.65	1.02	3.01	448.50	8.08	11.00	1.77	93	1.69
UC	UC_i1	Impact	108.75	25.60	2.03	51.59	2.91	1.11	2.39	707.64	5.37	21.00	2.19	53	1.09
	UC_i2	–	145.50	21.93	1.74	53.79	3.03	0.91	1.95	554.00	4.20	17.00	1.77	53	1.10
	UC_i3	–	154.88	22.79	1.81	52.63	2.97	0.86	1.86	553.11	4.20	18.00	1.88	48	0.99
	UC_i4	–	162.00	23.61	1.87	50.52	2.85	0.83	1.78	536.38	4.07	19.00	1.98	43	0.90
	Average	–	142.78	23.48	1.86	52.13	2.94	0.92	1.99	587.78	4.46	18.75	1.95	49	1.02
US	US_i1	Impact	100.28	18.84	1.74	44.65	2.60	1.24	2.82	629.56	7.06	16.00	1.88	77	1.50
	US_i2	–	133.08	19.66	1.82	48.39	2.81	0.95	2.15	565.22	6.34	16.00	1.88	59	1.14
	US_i3	–	153.75	20.76	1.92	50.79	2.95	0.84	1.92	544.92	6.11	15.00	1.76	56	1.09
	US_i4	–	158.40	19.91	1.84	48.02	2.79	0.81	1.85	476.16	5.34	17.00	2.00	48	0.92
	Average	–	136.38	19.79	1.83	47.96	2.79	0.96	2.19	553.96	6.22	16.00	1.88	60	1.16
UCNT	UCNT_i1	Impact	97.94	16.07	1.86	37.02	2.65	1.06	2.87	536.28	6.42	13.00	1.71	81	1.68
	UCNT_i2	–	121.62	14.62	1.69	37.68	2.69	0.99	2.69	536.90	6.42	14.00	1.84	71	1.46
	UCNT_i3	–	138.09	16.36	1.89	38.11	2.72	0.98	2.65	546.14	6.53	15.00	1.97	65	1.34
	Average	–	119.22	15.68	1.81	37.61	2.69	1.01	2.74	539.77	6.46	14.00	1.84	72	1.49

Table 6
The parameters related to the properties of FMZs of UM, UC, US, and UCNT [48].

Matrix	τ_{peak}		τ_{eq}		H	E	C-S-H	Porosity
	MPa	DIF	MPa	DIF	GPa	GPa	%	%
UM	20.31	1.88	14.65	1.18	2.30	42.30	69.30	5.12
UC	30.51	1.91	28.27	1.52	2.60	46.60	71.03	3.51
US	26.67	1.95	24.36	1.93	2.41	43.80	70.15	4.32
UCNT	20.80	2.06	16.79	1.95	2.32	42.80	69.40	4.57

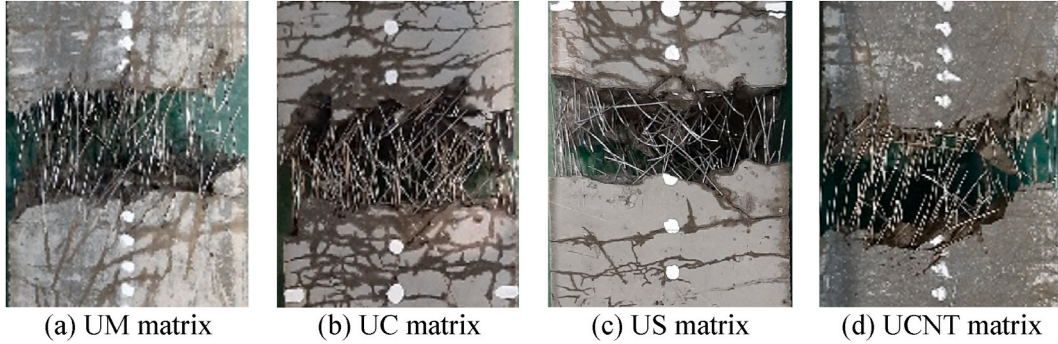


Fig. 10. Multiple cracking behaviors within the gauge length of matrices at high strain rates.

[41], Park et al. [26], and the experimental results obtained from this study. The curves produced using both the CEB-FIP and Malvar models from Eqs. (1) and (2) were unsuitable for estimating the DIFs of the post-cracking tensile strength of UHPFRC because they were based on the findings for conventional concrete under tension [40,42]. However, DIF calculated from the experimental test findings in this study closely matches the curve generated by the Park model in Eq. (3) [26] because the Park model is based on the test results for both FRC and UHPFRC containing smooth steel fibers.

Therefore, the prediction equations proposed by Park et al. [26] were considered appropriate for the matrices used in this study.

$$DIF_{pc} = \begin{cases} (\dot{\epsilon}/\dot{\epsilon}_s)^{1.1016\delta} & \text{for } \dot{\epsilon} \leq 30 \text{ s}^{-1} \\ \beta(\dot{\epsilon}/\dot{\epsilon}_s)^{1/3} & \text{for } \dot{\epsilon} > 30 \text{ s}^{-1} \end{cases} \quad (1)$$

$$DIF_{pc} = \begin{cases} (\dot{\epsilon}/\dot{\epsilon}_s)^\delta & \text{for } \dot{\epsilon} \leq 1 \text{ s}^{-1} \\ \beta(\dot{\epsilon}/\dot{\epsilon}_s)^{1/3} & \text{for } \dot{\epsilon} > 1 \text{ s}^{-1} \end{cases} \quad (2)$$

$$DIF_{pc} = \begin{cases} (\dot{\epsilon}/\dot{\epsilon}_s)^\delta & \text{for } \dot{\epsilon} \leq 25 \text{ s}^{-1} \\ \beta(\dot{\epsilon}/\dot{\epsilon}_s)^\eta & \text{for } \dot{\epsilon} > 25 \text{ s}^{-1} \end{cases} \quad (3)$$

where $\dot{\epsilon}$ denotes the applied strain rate; $\dot{\epsilon}_s$ indicates the static strain rate; $\delta = 1/(10 + 6f'_c/f'_{co})$, $1/(1 + 8f'_c/f'_{co})$, and $0.017-2722(f'_c/f'_{co})^{-7.33}$ in Eqs. (1)–(3), respectively; f'_c represents the static compression strength; $f'_{co} = 10 \text{ MPa}$; $\log \beta = 7.11 \delta - 2.33$, $6 \delta - 2$, and $-0.007082 - 2.08 f'_c$ in Eqs. (1)–(3), respectively; and $\eta = 0.1208 f'_c^{0.2622}$.

The rate-sensitive tensile resistance of the matrices can be attributed to the effects of the incubation time [43–46]. At lower strain rates, propagating cracks would have sufficient time to identify the route of least resistance; however, at high strain rates, cracks formed rapidly and did not have sufficient time to determine the weakest path. Therefore, they were pushed to propagate through the shortest route possible that contained elements with greater resistance, such as aggregates, resulting in an increased strength [43–46]. Furthermore, Rossi [47] reported that the existence of free water in the nanopores of cement hydrates is the primary cause of the increase in matrix strength at high strain rates. However, our investigation determined that the effects of free water were less significant in dry specimens. The source of the rate-sensitivity tensile parameters of UHPFRC is further discussed in Section 4.

4. Discussion

4.1. Effects of NPs on the tensile behavior of UHPFRC

The interfacial bond strength of fibers embedded in UHPFRC is crucial for enhancing their tensile resistance at high strain rates [10, 25,30,35]. Fig. 12 depicts the relationship between the post-cracking tensile strength and the interfacial bond strength of matrices at high strain rates. As illustrated in Fig. 12a, the post-cracking strength of UHPFRCs containing NPs increased significantly as the interfacial bond strength increased; however, the enhancement differed based on the type of NPs. Both post-cracking and interfacial

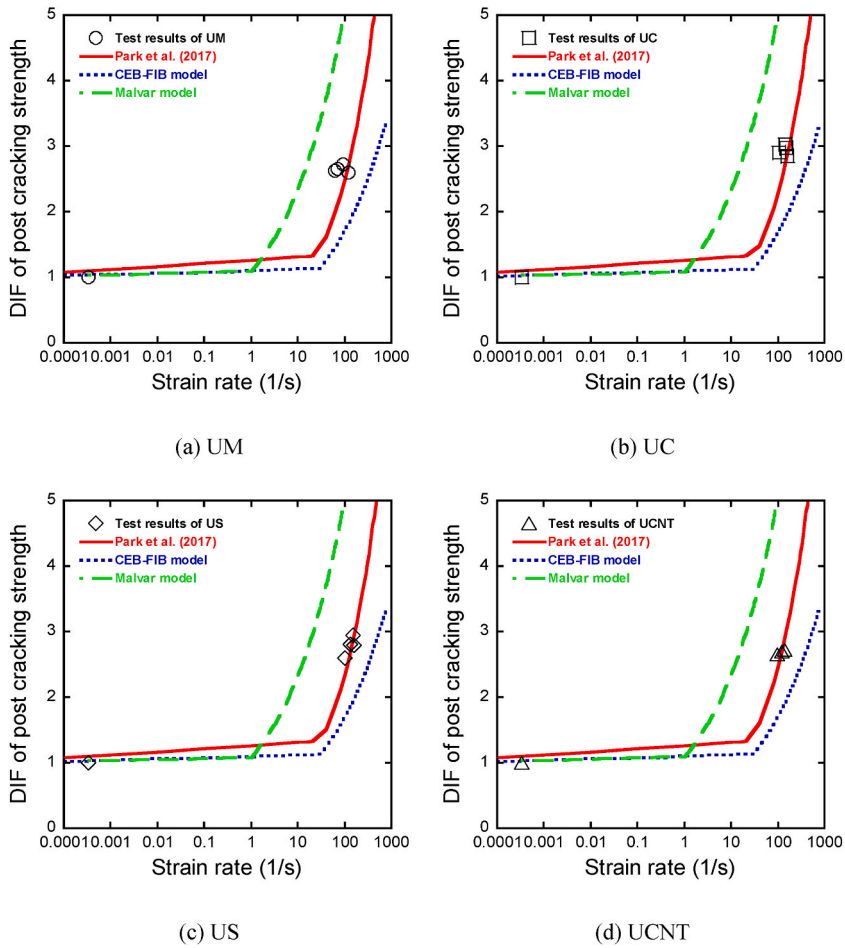


Fig. 11. Dynamic increase factors (DIFs) of the post-cracking tensile strength of matrices based on test results and predictive models.

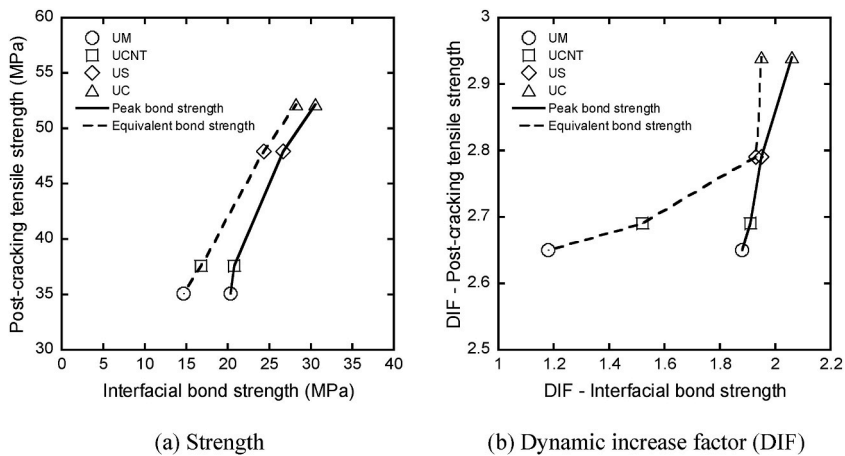


Fig. 12. Correlation between the post-cracking tensile strength and interfacial bond strength at high strain rates (Peak bond strength and equivalent bond strength are based on the data obtained from a previous study [48]).

bond strengths of the UC, US, and UCNT matrices were higher than those of the UM matrix. The post-cracking strengths of UC, US, UCNT, and UM matrices at high strain rates were 52.13, 47.96, 37.61, and 35.10 MPa, respectively, whereas the equivalent bond strengths of the matrices were 28.27, 24.36, 16.79, and 14.65 MPa, respectively (Fig. 12a). UHPFRC containing NPs produced higher

tensile resistance than the UM matrix owing to the highly optimized particle packing of NPs at the FMZ surrounding the fiber and matrix, which strongly adheres to the surface of the fibers and increases the interfacial bond strength.

The post-cracking strengths of the matrices were greater than the interfacial bond strengths. This can be attributed to the distribution of fibers, which produced various fiber inclination angles in the gauge lengths of the specimens, increasing the post-cracking strength. Park et al. [49] reported that the equivalent bond strength of smooth steel fibers embedded in UHPC increases significantly with the increase in the fiber inclination angle.

The rate-sensitive tensile resistances of the UHPFRC were highly correlated with the rate-sensitive pullout resistance of smooth steel fibers embedded in UHPC (Fig. 12b). As the rate-sensitive pullout resistance of matrices increased, their rate-sensitive tensile resistances also enhanced. For instance, the DIFs of equivalent bond strength of pullout impact tests increased from 1.18 to 1.95, while DIFs of the post-cracking strength of tensile impact tests were increased from 2.65 to 2.94, as shown in Fig. 12b. Section 4.2 explains the source of the rate-sensitivity tensile resistance of UHPFRC in detail.

Fig. 13 depicts the scanning electron microscope backscattered electron (SEM-BSE) images of the fiber–matrix zone (FMZ), which were identified in our previous research with an identical matrix composition, while Table 6 compares the parameters related to the properties of FMZs of matrices [48]. The FMZs of the matrices containing NPs (UC, US, and UCNT) had notably higher hardness (H) and Young's modulus (E) values than that of the UM matrix (without NPs), as provided in Table 6. The enhancement of both the H and E values was owing to their dense structure and/or enhanced hydration products caused by the NPs [15,22].

In addition, the matrices containing NPs generated lower porosity and higher homogeneity than the UM matrix, as shown in Fig. 13. The porosity area at FMZs of UC, US, UCNT, and UM was 3.51, 4.32, 4.57, and 5.12%, respectively, as provided in Table 6. Furthermore, the interfacial bond strengths of the matrices containing NPs were higher than those of UM. For instance, the peak bond strength (τ_{peak}) of UM, UC, US, and UCNT was 20.31, 30.51, 26.67, and 20.80 MPa, respectively, as listed in Table 6.

Matrices with higher compressive strengths are generally more sensitive to loading rates than matrices with lower compressive strengths [26,50]. Therefore, UC, US, and UCNT matrices with higher compressive strength generate higher rate-sensitive tensile resistance at high strain rates than the UM matrix. Furthermore, Park et al. [26] reported that UHPC with a higher matrix strength produces a higher tensile resistance than that with a lower matrix strength.

At the high strain rates, UHPFRC containing NPs exhibited lower rate-sensitive strain capacity than UM matrix, although UHPFRCs containing NPs produced higher compressive strength in comparison to UM matrix. This can be attributed to the crack widths of the UHPFRCs containing NPs being lower than that of UM matrix. For instance, although the UC matrix produced numerous multiple cracks, the crack width (49 μm) of the UC matrix was smaller than that of UM matrix (93 μm). Kim et al. [35] also investigated the rate-sensitive strain capacity of high-performance fiber-reinforced cementitious composites (HPFRCCs) corresponding to different matrix strengths (28, 56, and 84 MPa) at values ranging from pseudo-static (0.0001 s^{-1}) to seismic (0.1 s^{-1}) strain rates. They reported that the mortar matrix with 56 MPa compressive strength produced higher rate-sensitive strain capacity than that with 84 MPa compressive strength because the strain capacity was dependent upon not only matrix cracking strength but also interfacial bond strength. The relative enhancement of bond strength, in their study as the matrix strength increased, was relatively smaller than that in our study owing to the addition of NPs. The addition of NPs to UHPFRC slightly increased the compressive strength of matrices but significantly improved their interfacial bond strengths.

Additionally, the C–S–H property is another critical factor that affects the tensile behavior of UHPFRC. The addition of nano- CaCO_3 and nano- SiO_2 improved the C–S–H content of UHPFRCs, resulting in an increased rate-sensitive pullout resistance in the UHPFRCs [22,36]. The percentage of the C–S–H contents in the FMZs of UC, US were 71.03 and 70.15%, respectively, as provided in Table 6. Compared to the UM, the enhancement in the C–S–H content of UC was due to the nucleation effect of nano- CaCO_3 [22], whereas the improvement in the C–S–H content of US was attributed to the pozzolanic reaction of nano- SiO_2 [36]. Unlike nano- CaCO_3 and nano- SiO_2 , nano-CNTs only produced filling effects on the microstructure of the FMZ [37–39]. Therefore, UCNT did not exhibit a change in its C–S–H content. The C–S–H content of UCNT and UM matrices was 69.40 and 69.30%, respectively, as provided in Table 6.

4.2. Source of the rate-sensitive tensile resistance

The primary source of the rate-sensitive tensile behavior of UHPFRC is the interfacial bond and matrix strengths. The first-cracking strength primarily relies on the matrix strength, whereas the post-cracking strength, strain capacity, and peak toughness are closely associated with the interfacial bond strength.

4.2.1. Interfacial bond strength

Table 5 lists the DIFs of the post-cracking strengths of all matrices. Although the rate-sensitive tensile resistance of the matrices was dependent on the type of NPs, all matrices containing NPs produced greater DIFs of post-cracking strengths in comparison with the UM matrix. The DIFs of the post-cracking strength in the UC, US, UCNT, and UM matrices were 2.94, 2.79, 2.69, and 2.65, respectively (Table 5). The enhanced post-cracking strength of UHPFRC can be attributed to the characteristics of the interfacial bond strengths between the fibers and matrix, which are sensitive to the applied strain rate at high values.

The addition of NPs (nano- CaCO_3 , nano- SiO_2 , and nano-CNTs) to UHPFRC significantly increased the interfacial bond strength owing to the enhanced hardness (H) of the FMZ surrounding the fibers and matrix. The H of UHPFRCs containing NPs was higher than that of UM matrix. The H of UC, US, and UCNT was 2.60, 2.41, and 2.32 GPa, respectively, while that of UM was 2.30 GPa (Table 6). The addition of NPs to UHPFRCs enhanced the H of the FMZs because the NPs produced a high packing density of microstructures at FMZs and improve the C–S–H content of matrices. Furthermore, the adhesion and friction of straight fibers are primarily governed by the quantity of C–S–H and the density of the microstructure at the FMZs, consequently, the addition of NPs to UHPFRCs significantly increased the interfacial bond strengths of UHPFRCs [14,22]. Furthermore, the addition of nano- CaCO_3 and nano- SiO_2 to UHPFRC

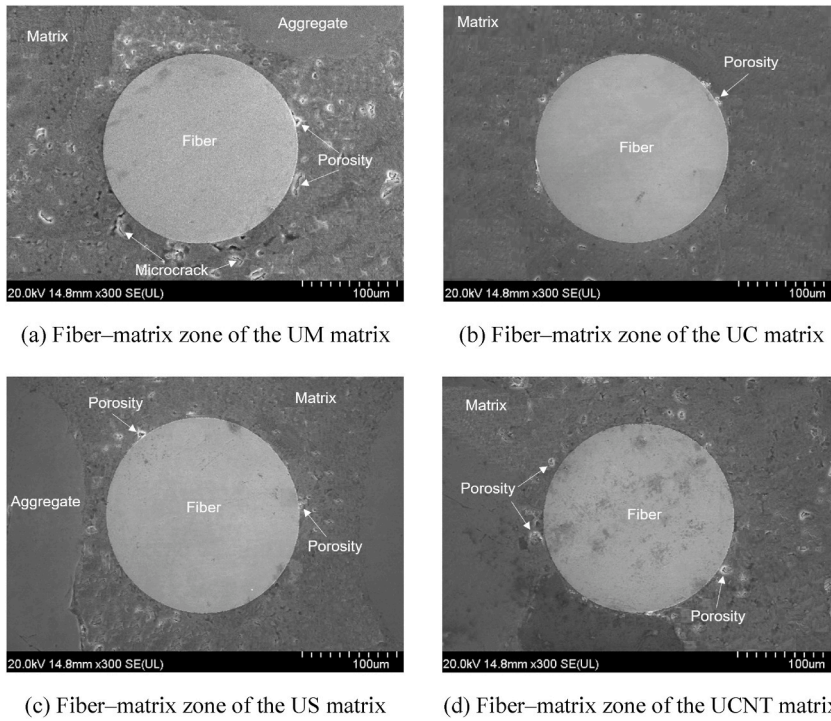


Fig. 13. Scanning electron microscope backscattered electron (SEM-BSE) images of fiber–matrix interfaces [48].

enhanced its microstructures and increased the content of C–S–H with a higher Ca/Si ratio [15,50]. Dang et al. [50] reported that matrices with higher Ca/Si ratios produce significantly higher rate sensitivity under loading rates. Unlike nano-CaCO₃ and nano-SiO₂, nano-CNT increased only the packing density of the UM matrix and not the C–S–H content owing to the filling effect, increasing the hardness of FMZs surrounding the fibers and matrix, consequently, the UCNT matrix generated a higher tensile rate sensitivity than the UM matrix [37–39].

Fig. 14 depicts the correlation between the hardness and interfacial bond strength, wherein the interfacial bond strengths of the matrices increased with the increase in the hardness of matrices. Among nano-CaCO₃, nano-SiO₂, and nano-CNT, nano-CaCO₃ produced the highest hardness (*H*) of the FMZ in the UC matrix, whereas nano-CNT exhibited the lowest hardness. The *H* values of the

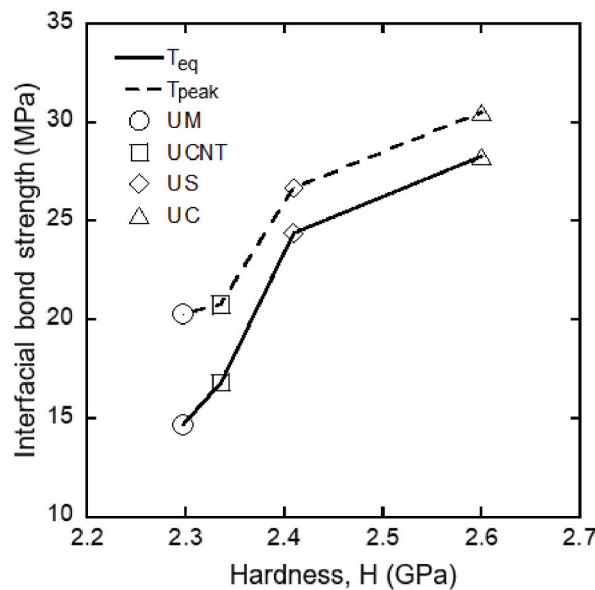


Fig. 14. Correlation between the hardness and interfacial bond strength.

FMZs corresponding to the UC, US, and UCNT matrices were 2.6, 2.41, and 2.32 GPa, respectively (Fig. 14). Therefore, the interfacial bond strengths, including τ_{peak} and τ_{eq} of the UC matrix, were higher than those of the US and UCNT matrices. The addition of nano-CaCO₃ to UHPFRC significantly increased the interfacial bond strength, enhancing the tensile resistance of the UC matrix at high strain rates in comparison with those of the US and UCNT matrices.

As indicated in Table 5, the strain capacities of all matrices increased considerably at high strain rates. The improved interfacial bond strength at high strain rates can increase both the post-cracking strength and strain capacity. This is because a higher interfacial bond strength generates more microcracks (Table 5). The strain capacity increased owing to the generation of a higher number of cracks, which increased the elongation within the gauge lengths. This trend of enhancement in the strain capacity with the increasing strain rate is consistent with the findings reported in the literature [10,26,27,30,51,52].

Table 5 and Fig. 7 indicate that the peak toughness of the matrices at higher strain rates was more than four times higher than that at the static strain rate. The enhanced energy absorption capacity at high strain rates can be attributed to the increased post-cracking strength and prolonged strain capacity at high strain rates. However, the interfacial bond strength between the fibers and matrices exhibits a significant influence on both the post-cracking strength and strain capacity [10]. Therefore, the energy-absorption capacity at high strain rates is primarily dependent on the interfacial bond strength of the matrices.

4.2.2. Matrix strength

The first-cracking strength (σ_{cc}) can be defined as the elastic modulus prior to cracking or the strain at first cracking [35]. This implies that the rate sensitivity of σ_{cc} primarily relies on the matrix strength [10]. UHPFRC containing NPs produced a higher rate sensitivity of first-cracking strength in comparison with UHPFRC without any NPs. The DIFs of σ_{cc} corresponding to the UC, US, UCNT, and UM matrices were 1.86, 1.83, 1.81, and 1.79, respectively (Table 5).

The higher rate sensitivity of σ_{cc} of UHPFRC containing NPs can be attributed to the higher compressive strength of the matrices because the addition of NPs to UHPFRC significantly increased the packing density on the microstructure of the matrices owing to the filling effects of the NPs. Furthermore, the addition of nano-CaCO₃ and nano-SiO₂ to UHPFRC enhanced the C–S–H content and changed the C–S–H structure with a higher Ca/Si ratio. Consequently, the rate sensitivity of the first-cracking strength of UHPFRC containing NPs was higher than that of UHPFRC without NPs.

5. Conclusions

This study investigated the effects of NPs on the tensile behavior of UHPFRC. Three types of NPs, namely nano-CaCO₃ (3 wt%), nano-SiO₂ (1 wt%), and nano-CNT (1 wt%) were used, and the tensile resistance of the UHPFRC was investigated at both static strain rate (0.000167 s⁻¹) and high strain rates (61.86–162.00 s⁻¹). The experimental findings and their implications can be summarized as follows.

- As the strain rates increased, all the UHPFRCs containing NPs exhibited rate-sensitive tensile resistance of the UHPFRCs. For instance, the DIF of post-cracking strengths of the UC, US, and UCNT matrices was 2.94, 2.79, and 2.69, respectively.
- The tensile rate-sensitivity of matrices was dependent on the types of NPs; UHPFRC containing nano-CaCO₃ (3%) produced higher DIFs of σ_{cc} , σ_{pc} , ϵ_{cc} , and T_p than the UHPFRC containing nano-SiO₂ (1%) or nano-CNT (1%) because nano-CaCO₃ produced higher rate-sensitive pullout resistance of smooth steel fibers in UHPFRC than other NPs.
- Among nano-CaCO₃, nano-SiO₂, and nano-CNT added to UHPFRC, nano-CaCO₃ generated the highest tensile strength of UHPFRC at high strain rates, whereas nano-CNT resulted in the lowest tensile strength. The enhancement of the post-cracking strength of UHPFRC containing nano-CaCO₃ at high strain rates was 48.53%, respectively, while that of UHPFRC containing nano-CNTs was 7.15%, respectively.
- The UC matrix with the UHPFRC containing nano-CaCO₃ (3 wt%) generated the lowest ϵ_{pc} (0.92%) at impact strain rates (108.75–162.00 s⁻¹), owing to their crack widths being smaller than those of other matrices.
- Finally, the primary source of the rate sensitivity of the post-cracking strength, number of microcracks, strain capacity, and peak toughness was identified to be the interfacial bond strength between the fiber and matrix. Additionally, the rate sensitivity of the first-cracking strength was primarily dependent on the matrix strength.

The study findings validate that the addition of NPs to UHPFRC containing long smooth steel fibers improves the rate-sensitive tensile resistance of the matrices. However, the influence of critical factors on the properties of UHPFRC, particularly the content of NPs, fiber type, fiber volume content, fiber distribution, fiber inclinations, and group effect of fibers, is not entirely clear. Further investigations are necessary to address these knowledge gaps.

Author statement

Van Phi DANG: Investigation, Writing- Original draft preparation. Dong Joo KIM: Methodology, Writing- Reviewing and Editing, Supervision.

Declaration of competing interest

The authors declare that they have no known competing financial interests or personal relationships that could have appeared to influence the work reported in this paper.

Data availability

Data will be made available on request.

Acknowledgments

This work was supported by the National Research Foundation of Korea (NRF), grant funded by the Korea government (MSIT) (Grant number 2022R1A2C2005234).

References

- [1] N.T. Tran, T.K. Tran, D.J. Kim, High rate response of ultra-high-performance fiber-reinforced concretes under direct tension, *Cement Concr. Res.* 69 (2015) 72–87, <https://doi.org/10.1016/j.cemconres.2014.12.008>.
- [2] A. Monaghan, *The Moscow Metro Bombings and Terrorism in Russia*, vol. 59, Research Division NATO Defence College, Rome, No. 2010, pp. 1–12.
- [3] E. Eskew, S. Jang, *Impacts and Analysis for Buildings under Terrorist Attacks*, *Environmental Engineering*, 2012.
- [4] V. Bindiganavile, N. Banthia, B. Aarup, Impact response of ultra-high-strength fiber-reinforced cement composite, *ACI Mater. J.* 99 (2002) 543–548, <https://doi.org/10.14359/12363>.
- [5] Y. Yao, F.A. Silva, M. Butler, V. Mechtcherine, B. Mobasher, Tensile and flexural behavior of ultra-high performance concrete (UHPC) under impact loading, *Int. J. Impact Eng.* 153 (2021), 103866, <https://doi.org/10.1016/j.ijimpeng.2021.103866>.
- [6] Homeland Security, Implementing 9/11 Commission Recommendations Progress Report 2011, U.S Department of Homeland Security, 2011, pp. 1–69. <https://www.dhs.gov/xlibrary/assets/implementing-9-11-commission-report-progress-2011.pdf>.
- [7] United Nations Office for Disarmament Affairs, Human Cost of Disasters, an Overview of the Last 20 Years 2000–2019, 2020, <https://doi.org/10.18356/79b92774-en>.
- [8] IEP, Global terrorism index 2022, Measuring the Impact of Terrorism, Institute for Economics & Peace, 2022. https://www.visionofhumanity.org/wp-content/uploads/2022/03/GTI-2022-web_110522-1.pdf.
- [9] N.T. Tran, T.K. Tran, J.K. Jeon, J.K. Park, D.J. Kim, Fracture energy of ultra-high-performance fiber-reinforced concrete at high strain rates, *Cement Concr. Res.* 79 (2016) 169–184, <https://doi.org/10.1016/j.cemconres.2015.09.011>.
- [10] T.K. Tran, D.J. Kim, Investigating direct tensile behavior of high performance fiber reinforced cementitious composites at high strain rates, *Cement Concr. Res.* 50 (2013) 62–73, <https://doi.org/10.1016/j.cemconres.2013.03.018>.
- [11] K. Wille, D.J. Kim, A.E. Naaman, Strain-hardening UHP-FRC with low fiber contents, *Mater. Struct.* 44 (2011) 583–598, <https://doi.org/10.1617/s11527-010-9650-4>.
- [12] K. Habel, M. Viviani, E. Denarié, E. Brühwiler, Development of the mechanical properties of an ultra-high performance fiber reinforced concrete (UHPFRC), *Cement Concr. Res.* 36 (2006) 1362–1370, <https://doi.org/10.1016/j.cemconres.2006.03.009>.
- [13] J.J. Buck, D.L. McDowell, M. Zhou, Effect of microstructure on load-carrying and energy-dissipation capacities of UHPC, *Cement Concr. Res.* 43 (2013) 34–50, <https://doi.org/10.1016/j.cemconres.2012.10.006>.
- [14] Z. Wu, K.H. Khayat, C. Shi, Effect of nano-SiO₂ particles and curing time on development of bond properties and microstructure of ultra-high strength concrete, *Cement Concr. Res.* 95 (2017) 247–256, <https://doi.org/10.1016/j.cemconres.2017.02.031>.
- [15] Z. Wu, C. Shi, K.H. Khayat, Multi-scale investigation of microstructure, fiber pullout behavior, and mechanical properties of ultra-high performance concrete with nano-CaCO₃ particles, *Cement Concr. Compos.* 86 (2018) 255–265, <https://doi.org/10.1016/j.cemconcomp.2017.11.014>.
- [16] N. Van Tuan, G. Ye, K. Van Breugel, O. Copuroglu, Hydration and microstructure of ultra high performance concrete incorporating rice husk ash, *Cement Concr. Res.* 41 (2011) 1104–1111, <https://doi.org/10.1016/j.cemconres.2011.06.009>.
- [17] C. Shi, Z. Wu, J. Xiao, D. Wang, Z. Huang, Z. Fang, A review on ultra high performance concrete: Part I. Raw materials and mixture design, *Construct. Build. Mater.* 101 (2015) 741–751, <https://doi.org/10.1016/j.conbuildmat.2015.10.088>.
- [18] D. Wang, C. Shi, Z. Wu, J. Xiao, Z. Huang, Z. Fang, A review on ultra high performance concrete: Part II. Hydration, microstructure and properties, *Construct. Build. Mater.* 96 (2015) 368–377, <https://doi.org/10.1016/j.conbuildmat.2015.08.095>.
- [19] W. Li, Z. Huang, F. Cao, Z. Sun, S.P. Shah, Effects of nano-silica and nano-limestone on flowability and mechanical properties of ultra-high-performance concrete matrix, *Construct. Build. Mater.* 95 (2015) 366–374, <https://doi.org/10.1016/j.conbuildmat.2015.05.137>.
- [20] K. Wille, K.J. Loh, Nanoengineering ultra-high-performance concrete with multiwalled carbon nanotubes, *Transport. Res. Rec.* 2142 (2010) 119–126, <https://doi.org/10.3141/2142-18>.
- [21] X.F. Liu, Q. Wang, X.Z. Duan, Y.X. Zhang, K.Q. Yu, Mechanical properties of nano-particle modified ultra-high performance fiber reinforced concrete, *Proceedings of the 25th Australasian Conference on Mechanics of Structures and Materials (ACMSM25)* 37 (2020) 449–454, https://doi.org/10.1007/978-981-13-7603-0_44.
- [22] Z. Wu, C. Shi, K.H. Khayat, S. Wan, Effects of different nanomaterials on hardening and performance of ultra-high strength concrete (UHSC), *Cement Concr. Compos.* 70 (2016) 24–34, <https://doi.org/10.1016/j.cemconcomp.2016.03.003>.
- [23] J. Moon, J.E. Oh, M. Balonis, F.P. Glasser, S.M. Clark, P.J.M. Monteiro, High pressure study of low compressibility tetracalcium aluminum carbonate hydrates 3CaO.AI₂O₃.CaCO₃.11H₂O, *Cement Concr. Res.* 42 (2012) 105–110, <https://doi.org/10.1016/j.cemconres.2011.08.004>.
- [24] F.U.A. Shaikh, T. Nishiwaki, S. Kwon, Effect of fly ash on tensile properties of ultra-high performance fiber reinforced cementitious composites (UHP-FRCC), *Journal of Sustainable Cement-Based Materials* 7 (2018) 357–371, <https://doi.org/10.1080/21650373.2018.1514672>.
- [25] A. Caverzan, E. Cadoni, M. Di Prisco, Tensile behaviour of high performance fibre-reinforced cementitious composites at high strain rates, *Int. J. Impact Eng.* 45 (2012) 28–38, <https://doi.org/10.1016/j.ijimpeng.2012.01.006>.
- [26] J.K. Park, S.W. Kim, D.J. Kim, Matrix-strength-dependent strain-rate sensitivity of strain-hardening fiber-reinforced cementitious composites under tensile impact, *Compos. Struct.* 162 (2017) 313–324, <https://doi.org/10.1016/j.compstruct.2016.12.022>.
- [27] T.K. Tran, N.T. Tran, D.J. Kim, Enhancing impact resistance of hybrid ultra-high-performance fiber-reinforced concretes through strategic use of polyamide fibers, *Construct. Build. Mater.* 271 (2021), 121562, <https://doi.org/10.1016/j.conbuildmat.2020.121562>.
- [28] N.T. Tran, D.J. Kim, Synergistic response of blending fibers in ultra-high-performance concrete under high rate tensile loads, *Cement Concr. Compos.* 78 (2017) 132–145, <https://doi.org/10.1016/j.cemconcomp.2017.01.008>.
- [29] S. Pyo, S. El-Tawil, A.E. Naaman, Direct tensile behavior of ultra high performance fiber reinforced concrete (UHP-FRC) at high strain rates, *Cement Concr. Res.* 88 (2016) 144–156, <https://doi.org/10.1016/j.cemconres.2016.07.003>.
- [30] S.H. Park, D.J. Kim, S.W. Kim, Investigating the impact resistance of ultra-high-performance fiber-reinforced concrete using an improved strain energy impact test machine, *Construct. Build. Mater.* 125 (2016) 145–159, <https://doi.org/10.1016/j.conbuildmat.2016.08.027>.
- [31] S.Y. Lee, H.V. Le, D.J. Kim, Self-stress sensing smart concrete containing fine steel slag aggregates and steel fibers under high compressive stress, *Construct. Build. Mater.* 220 (2019) 149–160, <https://doi.org/10.1016/j.conbuildmat.2019.05.197>.
- [32] K. Wille, S. El-Tawil, A.E. Naaman, Properties of strain hardening ultra high performance fiber reinforced concrete (UHP-FRC) under direct tensile loading, *Cement Concr. Compos.* 48 (2014) 53–66, <https://doi.org/10.1016/j.cemconcomp.2013.12.015>.
- [33] T.K. Tran, D.J. Kim, Strain energy frame impact machine (SEFIM), *J. Adv. Concr. Technol.* 10 (2012) 126–136, <https://doi.org/10.3151/jact.10.126>.
- [34] D. Kong, X. Du, S. Wei, H. Zhang, Y. Yang, S.P. Shah, Influence of nano-silica agglomeration on microstructure and properties of the hardened cement-based materials, *Construct. Build. Mater.* 37 (2012) 707–715, <https://doi.org/10.1016/j.conbuildmat.2012.08.006>.

- [35] D.J. Kim, S. El-Tawil, A.E. Naaman, Rate-dependent tensile behavior of high performance fiber reinforced cementitious composites, *Mater. Struct.* 42 (2009) 399–414, <https://doi.org/10.1617/s11527-008-9390-x>.
- [36] Z. Wu, K.H. Khayat, C. Shi, B.F. Tutikian, Q. Chen, Mechanisms underlying the strength enhancement of UHPC modified with nano-SiO₂ and nano-CaCO₃, *Cement Concr. Compos.* 119 (2021), 103992, <https://doi.org/10.1016/j.cemconcomp.2021.103992>.
- [37] M. Jung, Y.S. Lee, S.G. Hong, J. Moon, Carbon nanotubes (CNTs) in ultra-high performance concrete (UHPC): dispersion, mechanical properties, and electromagnetic interference (EMI) shielding effectiveness (SE), *Cement Concr. Res.* 131 (2020), 106017, <https://doi.org/10.1016/j.cemconres.2020.106017>.
- [38] S. Musso, J.M. Tulliani, G. Ferro, A. Tagliaferro, Influence of carbon nanotubes structure on the mechanical behavior of cement composites, *Compos. Sci. Technol.* 69 (2009) 1985–1990, <https://doi.org/10.1016/j.compscitech.2009.05.002>.
- [39] A. Chaipanich, T. Nochaiya, W. Wongkeo, P. Torkittikul, Compressive strength and microstructure of carbon nanotubes-fly ash cement composites, *Mater. Sci. Eng.* 527 (2010) 1063–1067, <https://doi.org/10.1016/j.msea.2009.09.039>.
- [40] Comite Euro-International du Beton, CEB-FIP Model Code 1990. Redwood Books, Thomas Telford Services Ltd., London, Trowbridge, Wiltshire, UK, 1993.
- [41] L.J. Malvar, C.A. Ross, Review of strain rate effects for concrete in tension, *ACI Mater. J.* 95 (1998) 735–739.
- [42] H.W. Reinhardt, Tensile fracture of concrete at high rates of loading, in: *Application of Fracture Mechanics to Cementitious Composites*, Springer, Netherlands, 1985, pp. 559–590, https://doi.org/10.1007/978-94-009-5121-1_20.
- [43] J.K. Park, T.T. Ngo, D.J. Kim, Interfacial bond characteristics of steel fibers embedded in cementitious composites at high rates, *Cement Concr. Res.* 123 (2019), 105802, <https://doi.org/10.1016/j.cemconres.2019.105802>.
- [44] L.B. Freund, *Dynamic Fracture Mechanics*, Cambridge University Press, New York, 1990.
- [45] A.J. Zielinski, Fracture of Concrete and Mortar under Uniaxial Impact Tensile Loading, Delft University of Technology, 1982. <http://resolver.tudelft.nl/uuid:07a0b5de-8835-4dfb-b271-7db6c352f0b6>.
- [46] Y.S. Tai, S. El-Tawil, T.H. Chung, Performance of deformed steel fibers embedded in ultra-high performance concrete subjected to various pullout rates, *Cement Concr. Res.* 89 (2016) 1–13, <https://doi.org/10.1016/j.cemconres.2016.07.013>.
- [47] P. Rossi, Strain rate effects in concrete structures: the LCPC experience, *Mater. Struct.* 30 (1997) 54–62, <https://doi.org/10.1007/bf02539277>.
- [48] V.P. Dang, D.J. Kim, Rate sensitive pullout resistance of smooth steel fibers embedded in ultra high performance concrete containing nano-particles, *Cement Concr. Compos.* (2022) (to be submitted).
- [49] J.K. Park, S.H. Park, D.J. Kim, Effect of matrix shrinkage on rate sensitivity of the pullout response of smooth steel fibers in ultra-high-performance concrete, *Cement Concr. Compos.* 94 (2018) 226–237, <https://doi.org/10.1016/j.cemconcomp.2018.09.014>.
- [50] V.P. Dang, H.V. Le, D.J. Kim, Loading rate effects on the properties of fiber-matrix zone surrounding steel fibers and cement based matrix, *Construct. Build. Mater.* 283 (2021), 122694, <https://doi.org/10.1016/j.conbuildmat.2021.122694>.
- [51] S. Pyo, K. Wille, S. El-Tawil, A.E. Naaman, Strain rate dependent properties of ultra high performance fiber reinforced concrete (UHP-FRC) under tension, *Cement Concr. Compos.* 56 (2015) 15–24, <https://doi.org/10.1016/j.cemconcomp.2014.10.002>.
- [52] K. Wille, S. El-Tawil, A.E. Naaman, Strain rate dependent tensile behavior of ultra-high performance fiber reinforced concrete, in: *High Performance Fiber Reinforced Cement Composites 6*, RILEM Bookseries, vol. 2, 2012, pp. 381–387, https://doi.org/10.1007/978-94-007-2436-5_46.